

Computer Methods in Biomechanics and Biomedical Engineering

ISSN: 1025-5842 (Print) 1476-8259 (Online) Journal homepage: <http://www.tandfonline.com/loi/gcmb20>

Validation of plantar pressure simulations using finite and discrete element modelling in healthy and diabetic subjects

W. Aerts, A. Scarton, F. De Groote, A. Guiotto, Z. Sawacha, C. Cobelli, J. Vander Sloten & I. Jonkers

To cite this article: W. Aerts, A. Scarton, F. De Groote, A. Guiotto, Z. Sawacha, C. Cobelli, J. Vander Sloten & I. Jonkers (2017): Validation of plantar pressure simulations using finite and discrete element modelling in healthy and diabetic subjects, Computer Methods in Biomechanics and Biomedical Engineering, DOI: [10.1080/10255842.2017.1372428](https://doi.org/10.1080/10255842.2017.1372428)

To link to this article: <http://dx.doi.org/10.1080/10255842.2017.1372428>



[View supplementary material](#)



Published online: 12 Sep 2017.



[Submit your article to this journal](#)



[View related articles](#)



[View Crossmark data](#)

Full Terms & Conditions of access and use can be found at
<http://www.tandfonline.com/action/journalInformation?journalCode=gcmb20>



Validation of plantar pressure simulations using finite and discrete element modelling in healthy and diabetic subjects

W. Aerts^a, A. Scarton^b, F. De Groote^c, A. Guiotto^b, Z. Sawacha^b, C. Cobelli^b, J. Vander Sloten^b and I. Jonkers^d

^aDepartment of Mechanical Engineering, Biomechanics Section, KU Leuven, Leuven, Belgium; ^bDepartment of Information Engineering, University of Padova, Padova, Italy; ^cDepartment of Mechanical Engineering, PMA, KU Leuven, Leuven, Belgium; ^dDepartment of Kinesiology, Human Movement Biomechanics, KU Leuven, Leuven, Belgium

ABSTRACT

Plantar pressure simulation driven by integrated 3D motion capture data, using both a finite element and a discrete element model, is compared for ten healthy and ten diabetic neuropathic subjects. The simulated peak pressure deviated on average between 16.7 and 34.2% from the measured peak pressure. The error in the position of the peak pressure was on average smaller than 4.2 cm. No method was more accurate than the other although statistical differences were found between them. Both techniques are thus complementary and useful tools to better understand the alteration of diabetic foot biomechanics during gait.

ARTICLE HISTORY

Received 6 June 2016
Accepted 23 August 2017

KEYWORDS

Gait analysis;
biomechanics; diabetes;
plantar pressure; discrete
element; finite element

1. Introduction

The prevalence of diabetes is increasing worldwide and is estimated to reach 4.4% by 2030 (Wild et al. 2004). People with diabetes, especially if affected by peripheral neuropathy, have 15–25% lifetime risk of developing a foot ulcer (Abbott et al. 2005; Singh et al. 2005) due to alterations in foot structure and function which lead to increased plantar pressure (PP) (van Schie 2005; Bennetts et al. 2013).

Investigation of the biomechanical factors contributing to the aforementioned alterations is crucial to improve treatment and prevention of diabetic neuropathic foot. Different techniques, both experimental and numerical, have been used for this purpose. On one side we find the external measurable variables that can be measured *in vivo*, like segmental movement, external forces and PP, on the other side we can find the numerical models (e.g. finite element models (FEMs)). Beside the advantage of the FEMs in term of the ability to provide insight into variables that cannot be measured *in vivo* like muscle forces or internal stresses and strains tolerated by the plantar tissue (Yarnitzky and Yizhar 2006), they are usually computational expensive and most commonly used for static or quasi-static loading simulations (Guiotto et al. 2014). Therefore in those cases where the interest could be limited to the estimation of PP such as for the design of therapeutic footwear and custom insoles for pressure relief (Lemmon et al. 1997; Chen et al. 2003;

Erdemir et al. 2006; Cheung and Zhang 2008; Oosterwaal et al. 2011) discrete element models (DEMs) can be used to model foot-ground contact in dynamic multibody gait simulations. This paper aim to propose an alternative to FEMs for predicting PP measures during dynamic conditions, thus overcoming limitations of the majority of current foot FEMs, and reducing costs associated to the experimental measurement set up.

This discrete element contact modelling is based on a small number of independent contact elements with a spring/damper-like behaviour and is commonly used to simulate ground reaction forces (GRF) (Wright et al. 1998; Neptune et al. 2000; Anderson and Pandy 2001; Ackermann and van den Bogert 2010). Although DEMs have been extensively assessed for simulating GRF, it has not yet been evaluated for simulating PP during gait. The mutual independency and the small number of contact elements allow fast contact simulations. Therefore this technique potentially allows to simulate the PP during dynamic situations.

The aim of this study was to evaluate the performance of FEM and DEM in simulating PP in control and diabetic subjects. The PP simulations were driven by integrated 3D motion capture data and the results are compared against measured PP. The analysis of model performance in both populations tests the sensitivity of both modelling approaches to the presence of diabetes and evaluates the potential use of both models in clinical practice.

2. Methods

2.1. Experimental data collection and preprocessing

Experimental 3D motion data was collected for ten healthy subjects (mean age 62.2 ± 4.60 years, mean BMI $24.6 \pm 2.16 \text{ kg/m}^2$) and ten diabetic neuropathic subjects (DNS) (mean age 63.2 ± 6.04 years, mean BMI $24.34 \pm 2.74 \text{ kg/m}^2$), suffering from peripheral neuropathy. The subjects were asked to walk barefoot at self-selected speed over a 10 m walkway using the marker placement protocol described in Sawacha et al. (2009, 2012). The 3D position of 30 retro-reflective markers was tracked at a sampling rate of 60 Hz using a six camera BTS stereophotogrammetric system (BTS S.r.l., Padova, Italy). GRF were recorded at 960 Hz using two Bertec force plates (FP4060-10, Bertec Corporation, Columbus, Ohio) embedded in the walkway. Simultaneously, PP was measured at 150 Hz using two pressure plate systems ($410 \times 410 \times 0.5 \text{ mm}$, 0.64 cm^2 resolution, 150 Hz, Imagortesi, Piacenza) mounted on top of the force plates. The study was approved by Padova University Hospital Ethics Committee and all participants gave written informed consent.

Experimental motion capture data were imported in the open-source software package OpenSim (Delp et al. 2007) to compute the input of both PP simulation methods more specific, the kinetic and kinematic boundaries for the FEM and the torque actuation driving a forward simulation for the DEM.

First the common workflow is described, followed by a description of the method-specific workflow in the next subsections. Gait simulations were based on a generic musculoskeletal model, 3DGaitModel2392 (Delp et al. 1990; Yamaguchi and Zajac 1989), consisting of 13 body segments and 23 degrees of freedom (DOFs). The ankle-foot complex is modelled with three segments: talus, foot (calcaneus, navicular, cuneiforms, cuboid and metatarsals) and toes (proximal and distal phalanges). These three segments are interconnected with three DOFs: flexion/extension in the ankle and metatarsophalangeal joints and a combination of eversion-abduction-extension/inversion-adduction-flexion in the subtalar joint. The generic musculoskeletal model was scaled to the subject's anthropometry using the marker data collected during a static trial. Thereafter, joint kinematics were calculated for each gait trial based on the measured marker trajectories (De Groote et al. 2008).

2.2. Discrete element model

Using DEM, the PP is calculated during a torque-driven multibody gait simulation. The contact modelling is

described first, followed by the multibody simulation workflow. The contact was simulated using independent discrete contact elements attached to each element of a triangular mesh of the foot surface. The triangular mesh used for all subjects, was generated from CT-images of one healthy foot (Mimics Innovation Suite, Materialise, Belgium). The mesh was divided in a 'foot mesh' (1920 elements) attached to the calcaneus and a 'toes mesh' (848 elements) attached to the toes, to be consistent with the two segment foot model in the multibody musculoskeletal model (Figure 1). The area of the triangular elements, which determines the resolution of the pressure simulation, was determined as such that it was close to or lower than the resolution of the pressure measurement system (0.64 cm^2). The area of the triangles in contact was on average 0.20 cm^2 with a standard deviation of 0.13 cm^2 . The contact geometry mesh was scaled together with the musculoskeletal model during the scaling step described above. The contact elements are spring-damper systems, relating the normal force (F_N) to the indentation (d) and indentation speed (\dot{d}) of the contact geometry with the simulated ground:

$$F_N = k d A (1 + c \dot{d}) \quad (1)$$

with k the stiffness per unit area, A the area of the contact element, and c the dissipation coefficient. Soft tissue is thus modelled as a visco-elastic material, where the stiffness coefficient k describes the elastic behaviour and the dissipation coefficient c the viscous behaviour. The tangential force component was calculated from the Stribeck friction function (Sherman et al. 2011) based on the slip velocity and the static, dynamic and viscous friction coefficient. As the contribution to the PP is mainly due to the normal force, the tangential force will not be discussed in the remainder of the section.

A torque-driven forward dynamic gait simulation was then generated for each subject based on 3D motion capture data (markers and GRF information). A Residual Reduction Algorithm (RRA) (Thelen and Anderson 2006) was applied based on the scaled model and computed joint kinematics in order to reduce the dynamic inconsistency between kinematics and experimental GRF resulting from modelling and measurement errors by slightly altering the model's kinematics and inertial properties. The remaining inconsistencies were accounted for by applying small residual forces and torques to the pelvis. Within RRA, the torque/force actuations for the different DOFs were calculated based on the measured GRF. These torque/force actuations were then used to drive the model in a forward simulation, using the DEM contact model. A closed-loop forward simulation was used, where a feedback loop based on the kinematic tracking error slightly

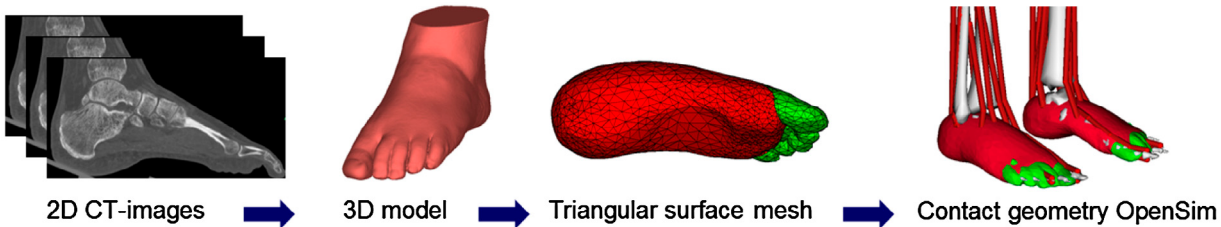


Figure 1. Workflow for constructing the triangular mesh, representing the location of the discrete contact elements. Starting from 2D CT-images a 3D model was constructed using the Mimics Innovation Suite (Materialise, Belgium). The sole of the 3D foot was separated of which a triangular mesh was generated. This mesh was divided into a ‘foot mesh’ and a ‘toes mesh’. The resulting meshes were added to the multibody musculoskeletal model.

adapted the torque/force actuations, to compensate for integration and modelling errors. The stiffness (k) and dissipation coefficient (c) of the contact model (as described above) and the contact geometry position with respect to the foot were calibrated by minimizing the feedback contributions to the driving forces and torques in the forward simulation. This optimization was performed automatically using an interior-point algorithm, implemented in C++ (SimTK, Simbody version 3.0). Between iterations the position of the contact geometry, the stiffness and damping coefficient were automatically adapted. The position of the contact geometry was calibrated to allow for small individual changes, such that a subject-specific contact geometry was not needed. The calibrated, and thus personalized, contact model was then used to calculate the PP distribution using the close-loop forward simulation. This PP distribution was determined based on the calculated force information of each individual contact element. Calibration of the contact parameters and the subsequent forward simulation were performed for each leg separately during stance. The GRF acting on the stance leg, was simulated based on the contact model, while for the other leg the measured GRF was used in the forward simulation (Figure 2). As only two force plates were used, complete information of the GRF was only available from the beginning of single-leg stance of the first leg in contact (right) till the end of single-leg stance of the second leg in contact (left). A visualization of a multibody forward simulation with a DEM PP simulation can be found in supplemental material.

2.3. Finite element model

Two type-specific FEMs were developed, based on MRI images (Philips Achieva and Siemens Avanto, 1.5T) of a foot of one healthy (HS-FEM) and one diabetic neuropathic subject (DNS-FEM) in unloaded conditions (Guittot et al. 2014). The plantar soft-tissue was represented as a continuum and its non-linear material

behaviour was modelled using an isotropic, nearly incompressible, hyperelastic second-order polynomial formulation. The stiffness coefficients for the DNS-FEM were increased by a factor of 2 with respect to those of the HS-FEM, in correspondence with Cheung and Zhang (2005). Four instants of the stance phase of gait were chosen to perform the finite element simulations: initial contact (IC, 1% of the stance), loading response (LR, first peak of the hindfoot vertical force), midstance (MS, minimum height of the markers of the foot from the floor) and push off (PO, peak of the forefoot vertical force) (Gefen et al. 2000). This choice allows covering the range of foot contact without performing a dynamic simulation.

Kinematics and kinetics acquired during the gait evaluations were used to define the boundary conditions of the FE simulations. The foot was placed relative to the plate according to the position acquired with the stereophotogrammetric system. The same anatomical landmarks adopted in the gait analysis protocol were identified on the skin surface of the FE model through virtual palpation. The reference system of the foot was created in Abaqus with the same rules adopted in Sawacha et al. (2009) and the 3D angles relatively to the global reference system were calculated. Then in the first step of each simulation the FE foot model was rotated in order to match the subject- and instant-specific position registered during the experimental data collection. In the second step, the plate was moved to get a first contact with the foot as done in Guiotto et al. (2014). Finally in the third step, the vertical joint contact force (JCF) was applied in the node corresponding to the midpoint between the lateral and the medial malleolus, according to the definition of the ankle coordinate system origin (Sawacha et al. 2009). This JCF at the ankle joint was calculated using the Joint Reaction analysis in OpenSim, with as input the scaled musculoskeletal model, calculated inverse kinematics and measured GRF. FE analyses were completed in Abaqus (Simulia, v.6.12).

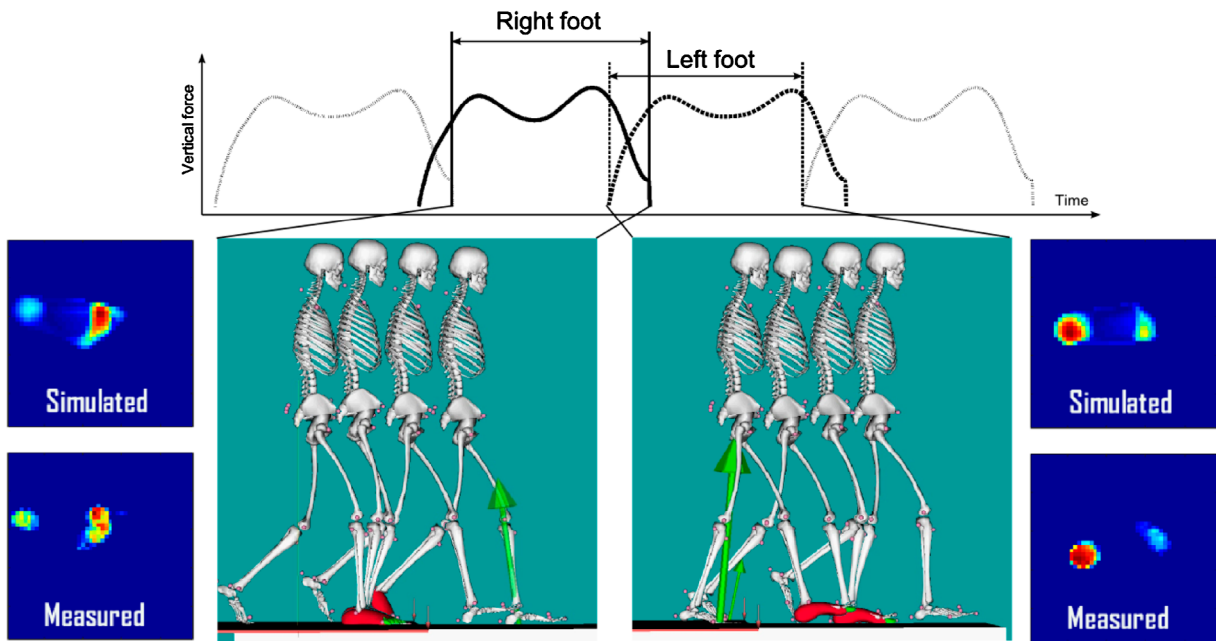


Figure 2. The contact optimization and PP simulation were performed for each foot separately during stance. Therefore the simulation of right foot contact started at toe-off of left foot, till toe-off of right foot. Simulation of left foot contact started at initial contact, till initial contact of right foot.

2.4. Statistical analysis

The simulated PP maps from both models were compared to the measured PP at four time instants by calculating the error between simulated and measured peak pressure magnitude and peak pressure location. The errors were calculated for the entire foot as a whole as well as for three subareas (hind-, mid- and forefoot). These subareas were automatically defined based on an anatomical landmark projection on the footprint (Sawacha et al. 2012) during mid stance (see Figure 3). The maps were expressed in a local foot axis definition as shown in Figure 3, in order to register the measured PP with those from the simulation (both FEM and DEM). The error on the peak pressure magnitude was normalized to the maximal measured peak pressure. The error on peak pressure location was normalized to foot length and foot width, respectively, for anterior-posterior and medio-lateral direction. Statistical analysis was performed to assess the difference between the simulated and experimental measured PP using a Wilcoxon signed-rank test. The statistical difference between the two models (DEM–FEM) and between the two groups (HS–DNS) was assessed using a non-parametric, two-sided Wilcoxon rank sum test, also called Mann-Whitney U-test. For all statistical analyses a significance level of 5% was used.

Table 1. Foot length, foot width and maximal measured peak pressure for the four different subareas, reported for the two groups (HS–DNS) (mean \pm SD).

	HS ^a	DNS ^a
Foot length	28.4 ± 1.89 cm	28.8 ± 1.92 cm
Foot width	10.6 ± 0.93 cm	10.8 ± 0.94 cm
Pmax foot	249.5 ± 6.0 kPa	248.6 ± 8.3 kPa
Pmax Forefoot	232.1 ± 21.8 kPa	239.9 ± 19.4 kPa
Pmax Midfoot	216.2 ± 36.4 kPa	213.4 ± 27.2 kPa
Pmax Hindfoot	208.8 ± 20.8 kPa	203.5 ± 23.2 kPa

^aNo statistical differences between the groups were found.

3. Results

Figure 4 shows the boxplot of the calibrated values of the stiffness (k) and dissipation (c) for the DEM for the healthy subjects and the diabetic patients. No statistical differences were found between the two groups, but a small trend of increased stiffness and decreased dissipation was found in the patient group. This latter group also showed a larger variation in stiffness and less variation in dissipation. The closed looped forward dynamics simulations of DEM resulted in sufficient low kinematic errors, with a maximal root mean square error of 6.27° and a maximal absolute error of 11.48° , calculated over all subjects and DOFs.

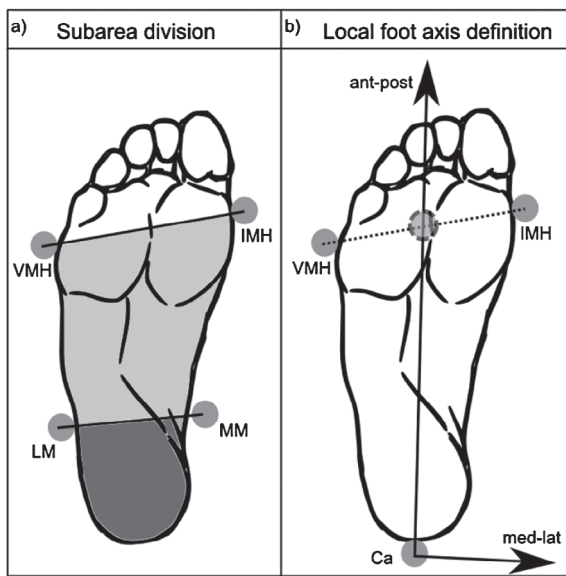


Figure 3. The foot was subdivided in 3 subareas (a). The subareas were hind-, mid- and forefoot and were determined based on anatomical landmark projection on the footprint during mid stance. The hind- and mid-foot subdivision was based on the lateral (LM) and medial (MM) malleoli markers. The mid- and forefoot were separated based on markers on the first (IMH) and fifth (VMH) metatarsal head. The peak pressure location was expressed in a local foot reference frame (b), defined based on projected marker information. The origin of this local reference frame was located at the projection of the calcaneus marker (Ca); the anterior-posterior axis was directed towards the middle of the metatarsal heads markers; and the medio-lateral axis was perpendicular to the anterior-posterior axis.

Table 1 reports the mean maximal measured peak pressure, foot length and foot width over the ten healthy and diabetic subjects. These values were used to normalize the difference between simulated and measured pressure magnitude and location. No statistical differences were found between the two groups. A slightly lower maximal peak pressure is found for the hindfoot compared to the forefoot.

Figure 5 represents the errors between the simulated and the corresponding measured peak pressure over the ten subjects, grouped per model (DEM–FEM) and population (HS–DNS). The simulated peak pressure were found to be statistical different from the measured peak pressure for both methods, except for the DEM at PO and at LR (for hindfoot) and for both FEM and DEM at IC. The values of mean, minima and maxima of the absolute errors are given in Table 2. It can be seen that on average the absolute error is relatively small: 16.7%/22.8% (DEM–HS/DNS) and 34.2%/32.3% (FEM–HS/DNS) for DEM and FEM, respectively. Maximal deviation is about 50% of maximal measured peak pressure, corresponding to a deviation of 125kPa. Figure 6 visualizes the error in simulated peak pressure location for the anterior-posterior

direction and Figure 7 for the medio-lateral direction. The error is in most cases smaller than 15% of the foot length (± 4.2 cm), except for the whole foot at MS and for the mid-foot at LR, where the error reaches up to 50% of the foot length. The relative error in the medio-lateral direction (Figure 7) was slightly larger than the error in the anterior-posterior direction, with values up to 50% of the foot width (± 5 cm) with a large variability in both magnitude and sign of the error.

A significant difference in peak pressure between the two models (DEM–FEM) was found for almost all time instants and subareas. The DEM mainly underestimated the peak pressure, whereas the FEM tended to overestimate the peak pressure at LR, but underestimated the peak pressure at PO. However the error magnitude is found to be similar for both FEM and DEM. The peak pressure location in anterior-posterior direction reveals statistical difference between the two models for the healthy subjects at LR and MS and for the diabetic patients at MS, PO and IC. Less statistical differences were observed for the peak pressure location in medio-lateral direction, only for the healthy subjects at IC and MS (forefoot) and for the diabetic group at PO.

A significant difference in peak pressure between the two groups (HS–DNS) was only found for the FEM at LR (mid-foot) and at MS (whole foot). In addition a statistically different anterior-posterior peak pressure location was found for the FEM at LR, MS and PO, and for the DEM at LR. The medio-lateral direction was only significantly different for the DEM at LR (mid-foot).

4. Discussion

This study compares two different techniques for simulating PP based on 3D motion capture data, for both healthy subjects and diabetic patients. A first technique is based on a DEM, where the contact is simulated using independent contact elements, attached to a musculoskeletal model. The second approach is based on a state-of-the-art FEM of the foot, where the contact is simulated quasi-statically at discrete time instances of stance. For both methods the 3D motion capture data, consisting of GRF and marker trajectories, is used as input and the measured PP is used for validation. The error on the peak pressure and peak pressure location showed that the DEM performs comparably well compared to the FEM. Although statistical differences were found between the two models, in general, no model outperforms the other. The magnitude and the direction of the error are variable depending on the time instant and subarea studied. Nevertheless, DEM tended to slightly underestimate the magnitude of peak pressure was found for DEM, whereas the FEM tended to overestimate the magnitude

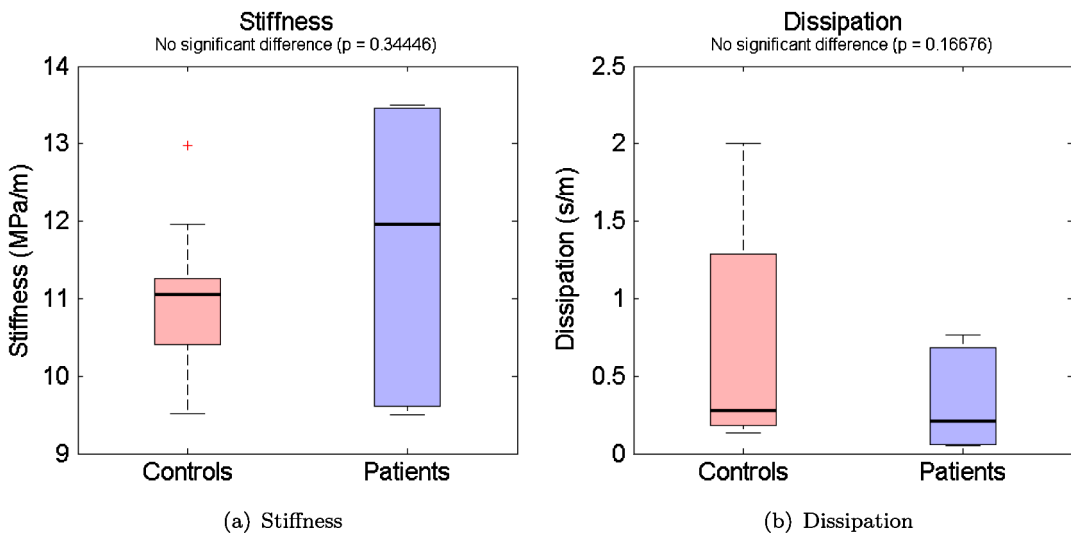


Figure 4. Boxplot of the calibrated values for the stiffness (a) and the dissipation (b), for both the healthy control and diabetic patient group. Box-plots show median, 25–75 percentiles, min–max values and outliers. An unpaired t-test is performed to test for statistical differences.

Table 2. Mean, minima and maxima of the absolute error on the simulated peak pressure over the ten subjects is shown as a percentage of the maximal measured pressure.

	HS						DNS					
	DEM			FEM			DEM			FEM		
	mean	min	max	mean	min	max	mean	min	max	mean	min	max
<i>Foot</i>												
LR	13.45	1.87	25.18	24.68	1.70	53.11	13.57	0.47	39.23	22.10	6.46	39.47
MS	15.80	0.08	37.72	32.52	15.29	47.43	18.41	2.99	48.77	18.00	0.67	39.33
PO	9.02	1.10	20.01	39.49	8.86	63.06	10.95	0.07	23.69	39.62	23.13	58.64
IC	27.59	4.51	54.55	28.54	1.36	61.28	40.98	14.74	81.33	17.04	3.84	36.77
<i>Forefoot</i>												
MS	11.09	0.76	31.36	35.34	13.51	56.35	25.88	6.79	62.28	37.31	6.86	74.24
PO	8.28	1.10	18.95	38.31	10.27	60.18	16.08	0.07	67.17	43.15	19.05	65.67
<i>Midfoot</i>												
LR	18.99	1.68	39.19	26.93	3.42	55.25	19.53	5.11	39.53	48.42	14.76	64.71
MS	20.06	4.39	42.71	54.11	40.34	67.04	16.84	2.99	40.20	49.29	1.26	74.74
<i>Hindfoot</i>												
LR	14.08	2.41	23.28	32.25	6.11	63.04	18.20	0.62	39.23	27.62	8.08	48.29
IC	28.79	4.95	54.80	29.90	1.47	67.35	47.59	22.25	81.33	20.35	3.97	40.97
Average	16.72	2.29	34.78	34.21	10.23	59.41	22.80	5.61	52.28	32.29	8.81	54.28

Notes: The errors are shown for all combination of group (HS–DNS) and model (DEM–FEM): DEM–HS, FEM–HS, DEM–DNS, FEM–DNS. The row shows the subdivision in the three different subareas and total foot and the four discrete time instants. The last row is the averaged mean, minimum and maximum error for the different combination of group and model.

of the peak pressure at LR, but to underestimate the magnitude of peak pressure at PO.

Both models perform comparable well for both healthy and diabetic patient group, with a non-significant different error found between the two groups. Only a significant difference between the two groups was found for the DEM at LR (peak pressure location) and for the FEM at LR (mid-foot) and at MS (whole foot). For the FEM these differences could be explained by the use of two type-specific FEMs with different soft-tissue prop-

erties and foot geometry according to the population under analysis. It is shown that the model for the healthy subjects outperforms the one of the diabetic patients at LR and at PO for peak pressure and anterior-posterior peak pressure location, while the reverse is true at MS. The DEM on the other hand uses the same contact geometry for both HS and DNS, but the contact parameters and geometry position were calibrated to maximize the correspondence with the measured GRF. Although no statistical differences were found, the calibration results

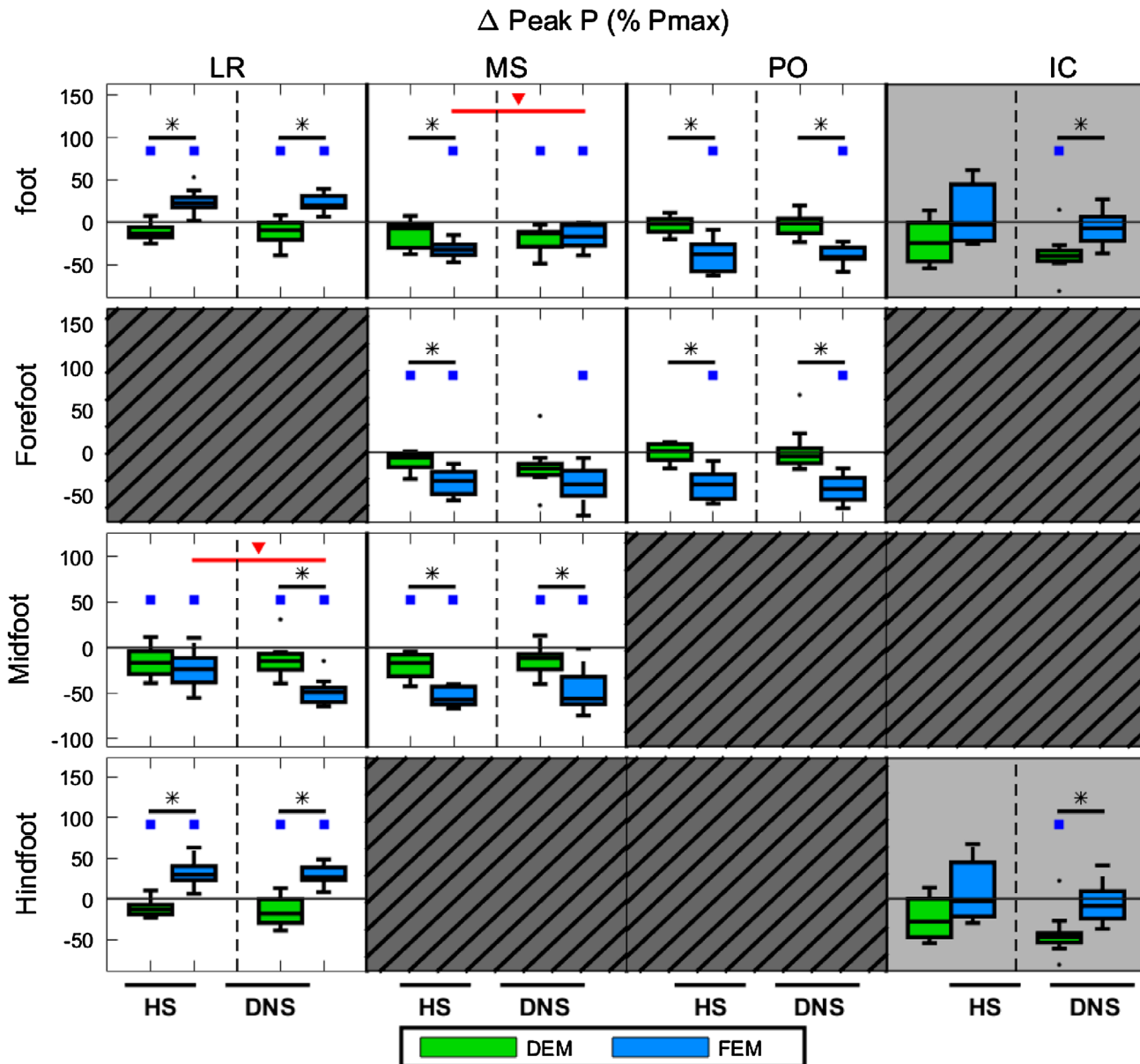


Figure 5. Difference between simulated and measured peak pressure as a percentage of the maximal measured pressure. A positive value represents an overestimation of the peak pressure, while a negative value represents an underestimation. The results were calculated at four discrete time instants (columns) and for total foot and three different subareas (rows). IC was simulated for the bilateral side (gray infilled plot). Per time instant and per subarea, four boxplots are shown for each combination of group (HS–DNS) and model (DEM–FEM): DEM–HS, FEM–HS, DEM–DNS and FEM–DNS, respectively. These boxplots were calculated over the ten subjects per group, indicating the median, first/third quartiles and minimum/maximum value. A square (□) above the boxplot indicates a statistical difference between simulation and measurement. Statistical significant differences between groups (HS–DNS) are indicated by a triangle (▽) and significant differences between models (DEM–FEM) are indicated by an asterisk (*). Only results with contact of the relevant foot parts are presented.

revealed a small trend of increased stiffness and decreased dissipation for the patients group. This is in correspondence with recent indentation studies (Jan et al. 2013; Chatzistergos et al. 2014). Jan et al. (2013) found an increase of 300% of the effective Young's modulus at the first metatarsal head for diabetic patients, while Chatzistergos et al. (2014) reported an increase of 50% of the stiffness. In the latter study decreased energy absorption is found, which is related to the dissipation in the soft tissue. This confirms the observed decrease of the

dissipation parameter in our DEM contact model. The larger variability of the stiffness parameter for the patients group, might be related to the difference in diabetes involvement. Due to the parameter calibration the DEM approach resulted in less statistical differences between groups (HS–DNS) and hence better correspondence with the differences observed based on the measured PP of both healthy and diabetic subjects.

The simulation differences found in this study are comparable to other finite element studies (Chen et al.

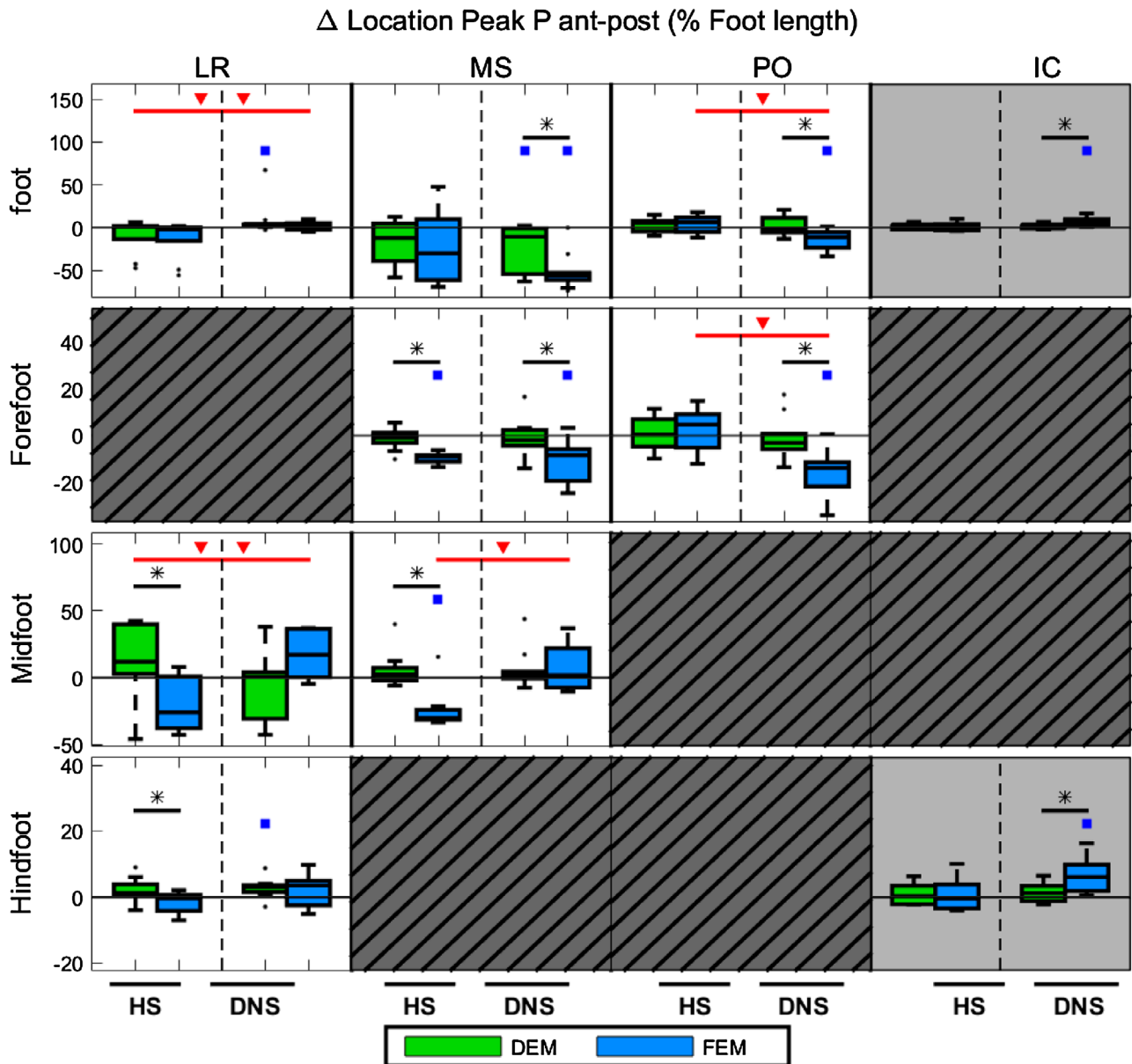


Figure 6. Difference between simulated and measured peak pressure location in the anterior-posterior direction is shown as a percentage of the foot length. A positive value represents an error in anterior direction, while a negative value is an error in posterior direction. The results were calculated at four discrete time instants (columns) and for total foot and three different subareas (rows). IC was simulated for the bilateral side (gray infilled plot). Per time instant and per subarea, four boxplots are shown for each combination of group (HS–DNS) and model (DEM–FEM): DEM–HS, FEM–HS, DEM–DNS and FEM–DNS, respectively. These boxplots were calculated over the ten subjects per group, indicating the median, first/third quartiles and minimum/maximum value. A square (□) above the boxplot indicates a statistical difference between simulation and measurement. Statistical significant differences between groups (HS–DNS) are indicated by a triangle (∇) and significant differences between models (DEM–FEM) are indicated by an asterisk (*). Only results with contact of the relevant foot parts are presented.

2010; Cheung and Zhang 2005; Actis et al. 2006; Erdemir et al. 2006; Fernandez et al. 2012; Guiotto et al. 2014). However, most of these state-of-the-art finite element simulations are limited to a static simulation of quiet standing, except for two studies, where they simulate at IC, MS and PO, an approach comparable to the current study (Fernandez et al. 2012; Guiotto et al. 2014). In addition, these FEM studies typically used a personalized

model of the foot, retrieved from imaging techniques. However in this study a general type-specific model is used, which may explain the larger error found compared to other studies (Fernandez et al. 2012). In this study both models used a general (type-specific) contact geometry for all subjects, reducing significantly the time cost for running PP simulation for larger populations. It eliminates the time needed for medical image processing

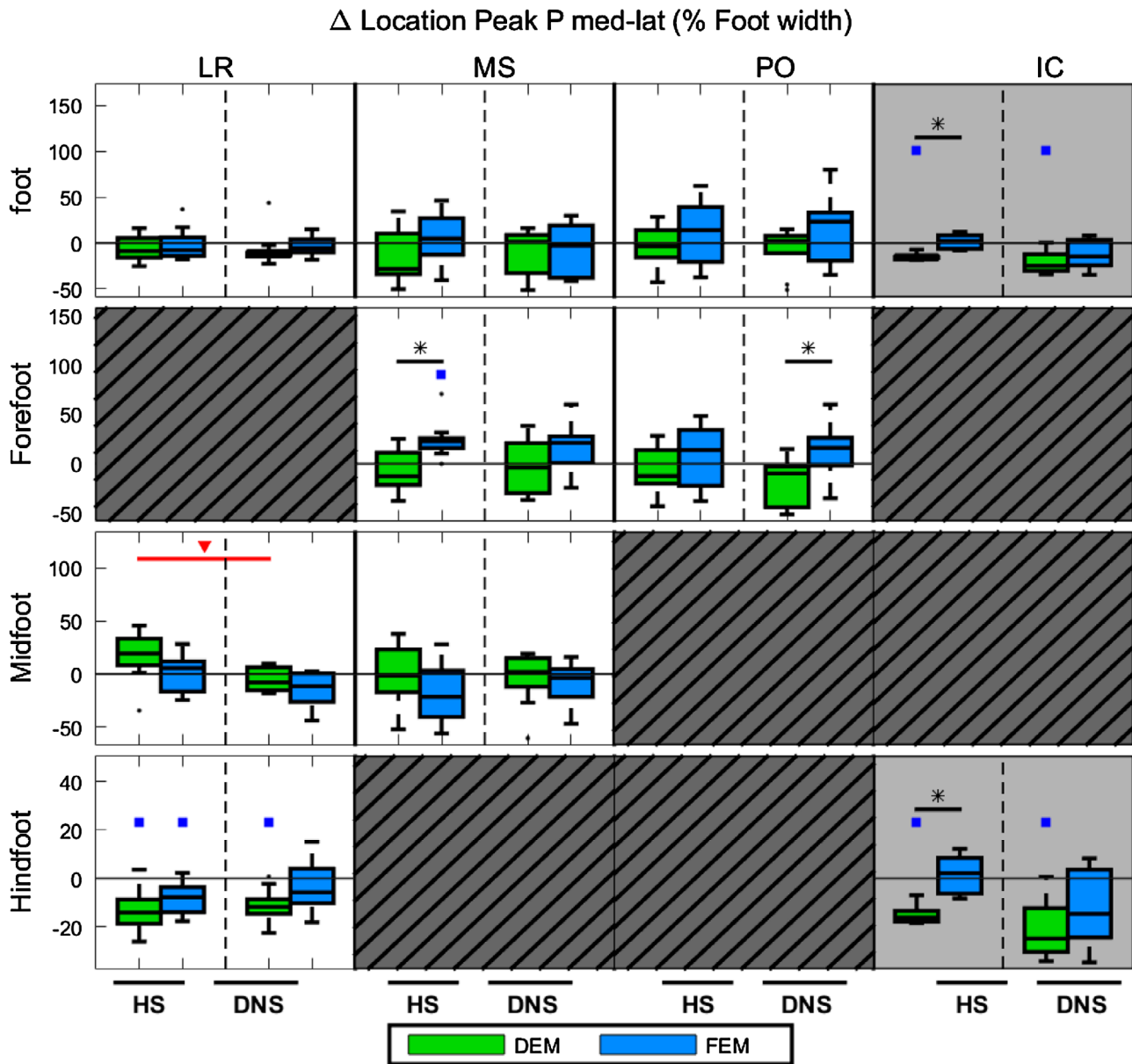


Figure 7. Difference between simulated and measured peak pressure location in the medio-lateral direction as a percentage of the foot width. A positive value represents an error in medial direction, while a negative value is an error in lateral direction. The results are calculated at four discrete time instants (columns) and for total foot and three different subareas (rows). IC was simulated for the bilateral side (gray infilled plot). Per time instant and per subarea, four boxplots are shown for each combination of group (HS–DNS) and model (DEM–FEM): DEM–HS, FEM–HS, DEM–DNS and FEM–DNS, respectively. These boxplots are calculated over the ten subjects per group, indicating the median, first/third quartiles and minimum/maximum value. A square (\square) above the boxplot indicates a statistical difference between simulation and measurement. Statistical significant differences between groups (HS–DNS) are indicated by a triangle (∇) and significant differences between models (DEM–FEM) are indicated by an asterisk (*). Only results with contact of the relevant foot parts are presented.

(CT or MRI) and subject-specific model construction. Despite the use of this general geometry, we were able to produce similar simulation results as found in literature.

For using PP in insole prescription for PP relief the fact that a technique produce an overestimate can be compatible with the need of pressure relief. Secondly the possibility of providing an overall PP analysis for plan-

ning PP relief insoles or orthosis will reduce costs associated with both PP measurement devices and foot orthosis or insoles samples productions as already demonstrated in the literature (Lemmon et al. 1997; Chen et al. 2003; Erdemir et al. 2006; Cheung and Zhang 2008; Oosterwaal et al. 2011). This will positively impact on the diffusion of PP based foot orthosis prescription which has already

been shown to represent a better solution in diabetic foot prevention (Bus et al. 2013; Erdemir et al. 2005). Future efforts should be put on improving both FEMs and DEMs by adding subject-specific material properties to the simulations.

Both models have their own advantages and limitations. FEM allows biofidelic modelling of all components of the foot and allows retrieving information on the internal stresses and strains. These mechanical stress concentrations in deep tissues of the plantar pad are found to play a dominant role in the mechanism of DNS's foot injuries and may lead to foot ulceration (Cavanagh et al. 1993; Erdemir et al. 2005; Yarnitzky and Yizhar 2006). However, FEM results in models with large number of elements and this makes the method computational expensive. Therefore it is commonly used in static or quasi-static loading situations, for a subset of poses of the gait cycle. The DEM allows a continuous PP simulation with a limited time cost of five minutes for a whole gait cycle. Therefore this method is suitable for dynamically evaluating new alternative designs of therapeutic insoles or customized footwear as they require numerous simulations. However, due to the one-dimensionality of the contact elements, this method is not able to retrieve information on the internal stresses and strains, which can be derived using the FEM. The reported time cost is only the cost of simulation of one gait cycle and does not take into account the time needed for calibration of the DEM. The duration of this calibration process is on average one day, but only needs to be done once per subject and can therefore be easily used for different trials or for simulations with insoles.

Further improvements of the FEM could be achieved by including the muscle forces in the FE simulations which can be estimated by means of OpenSim. It has been reported that diabetic and healthy subjects differ in muscle activation and strength during motion (Andersen et al. 1996). Muscle forces play a really predominant role in the different steps of the gait cycle thus they need to be considered (Chen et al. 2010).

The DEM could be improved by refining the underlying multibody musculoskeletal model. In this study, a two-segment foot model is used, but further research is needed to develop and validate a more advanced foot model with additional degrees of freedom. In addition, non-linear contact parameters can be implemented, in order to mimic the non-linear soft-tissue behaviour. This would further improve the contact simulation for highly-dynamic situations such as during initial contact. It is also possible to personalize the DEM by including a subject-specific mesh of the foot and attributing stiffness and damping values for each triangular element of the mesh

separately, based on the soft tissue thickness. The time cost for personalization of the DEM, is estimated to be less than the cost for a personalized FEM.

5. Conclusion

To our knowledge, this is the first study evaluating a DEM for the simulation of PP. The DEM was compared with a finite element simulation for ten healthy subjects and ten diabetic neuropathic patients. Although statistical differences were found between the two models, both performed comparably for the peak pressure magnitude and location simulation. A tendency of slight underestimation of peak pressure was found for DEM at loading response and mid-stance, whereas the FEM tended to overestimate the peak pressure at loading response, but to underestimate the peak pressure at push-off. The DEM allows a continuous dynamic PP simulation with a limited time cost of five minutes for a whole gait cycle. The FEM on the other hand can provide additional information on the internal stress distribution in the soft tissue. Both models are thus complementary, which makes it possible to enhance the insight in the diabetic foot biomechanics, and hence to improve the prevention of plantar ulcer formation.

Acknowledgements

We acknowledge Prof Angelo Avogaro and Dr Gabriella Guarneri for their participation in the original collection of the dataset; Imagortesi, Piacenza for providing the plantar pressure system.

Disclosure statement

No potential conflict of interest was reported by the authors.

Funding

Funding for this study was provided by the Materialise Chair for Image Based, Patient-Specific Biomechanics and the Agency for Innovation by Science and Technology (IWT) [grant number 131040].

References

- Abbott CA, Garrow AP, Carrington AL, Morris J, Van Ross ER, Boulton AJ. 2005. Foot ulcer risk is lower in South-Asian and African-Caribbean compared with European diabetic patients in the U.K.: the North-West diabetes foot care study. *Diabetes Care*. 28(8):1869–1875.
- Ackermann M, van den Bogert AJ. 2010. Optimality principles for model-based prediction of human gait. *J Biomech*. 43(6):1055–1060. DOI:[10.1016/j.jbiomech.2009.12.012](https://doi.org/10.1016/j.jbiomech.2009.12.012)
- Actis RL, Ventura LB, Smith KE, Commean PK, Lott DJ, Pilgram TK, Mueller MJ. 2006. Numerical simulation of the

- plantar pressure distribution in the diabetic foot during the push-off stance. *Med Biol Eng Comput.* 44(8):653–663.
- Andersen H, Poulsen PL, Mogensen CE, Jakobsen J. **1996 Apr.** Isokinetic muscle strength in long-term IDDM patients in relation to diabetic complications. *Diabetes.* 45:440–445.
- Anderson FC, Pandy MG. **2001 Oct.** Dynamic optimization of human walking. *J Biomech Eng.* 123:381–390.
- Bennetts CJ, Owings TM, Erdemir A, Botek G, Cavanagh PR. **2013.** Clustering and classification of regional peak plantar pressures of diabetic feet. *J Biomech.* 46(1):19–25. DOI:[10.1016/j.jbiomech.2012.09.007](https://doi.org/10.1016/j.jbiomech.2012.09.007)
- Bus SA, Ulbrecht JS, Cavanagh PR. **2013.** Pressure relief and load redistribution by custom-made insoles in diabetic patients with neuropathy and foot deformity. *Clin Biomech.* 19(6):629–638. DOI:[10.1016/j.clinbiomech.2004.02.010](https://doi.org/10.1016/j.clinbiomech.2004.02.010)
- Cavanagh PR, Simoneau GG, Ulbrecht JS. **1993.** Ulceration, unsteadiness, and uncertainty: the biomechanical consequences of diabetes mellitus. *J Biomech.* 26(Suppl 1):23–40.
- Chatzistergos PE, Naemi R, Sundar L, Ramachandran A, Chockalingam N. **2014.** The relationship between the mechanical properties of heel-pad and common clinical measures associated with foot ulcers in patients with diabetes. *J Diabetes Complications.* 28(4):488–493. DOI:[10.1016/j.jdiacomp.2014.03.011](https://doi.org/10.1016/j.jdiacomp.2014.03.011)
- Chen WM, Lee T, Lee PVS, Lee JW, Lee SJ. **2010.** Effects of internal stress concentrations in plantar soft-tissue – a preliminary three-dimensional finite element analysis. *Med Eng Phys.* 32(4):324–331. DOI:[10.1016/j.medengphy.2010.01.001](https://doi.org/10.1016/j.medengphy.2010.01.001)
- Chen WP, Ju CW, Tang FT. **2003.** Effects of total contact insoles on the plantar stress redistribution: a finite element analysis. *Clin Biomech.* 18:S17–S24.
- Cheung JTM, Zhang M. **2005 Feb.** A 3-dimensional finite element model of the human foot and ankle for insole design. *Arch Phys Med Rehabil.* 86:353–358.
- Cheung JTM, Zhang M. **2008.** Parametric design of pressure-relieving foot orthosis using statistics-based finite element method. *Med Eng Phys.* 30:269–277.
- De Groote F, De Laet T, Jonkers I, De Schutter J. **2008.** Kalman smoothing improves the estimation of joint kinematics and kinetics in marker-based human gait analysis. *J Biomech.* 41:3390–3398.
- Delp SL, Anderson FC, Arnold AS, Loan P, Habib A, John CT, Guendelman E, Thelen DG. **2007.** OpenSim: open-source software to create and analyze dynamic simulations of movement. *IEEE Trans Biomed Eng.* 54(11):1940–1950.
- Delp SL, Loan P, Hoy MG, Zajac FE, Topp EL, Rosen JM. **1990.** An interactive graphics-based model of the lower extremity to study orthopaedic surgical procedures. *IEEE Trans Biomed Eng.* 37(8):757–767.
- Erdemir A, Saucerman JJ, Lemmon D, Lopponow B, Turso B, Ulbrecht JS, Re Cavanagh P. **2005.** Local plantar pressure relief in therapeutic footwear: design guidelines from finite element models. *J Biomech.* 38(9):1798–1806.
- Erdemir A, Viveiros ML, Ulbrecht JS, Cavanagh PR. **2006.** An inverse finite-element model of heel-pad indentation. *J Biomech.* 39:1279–1286.
- Fernandez JW, Ul Haque MZ, Hunter PJ, Mithraratne K. **2012.** Mechanics of the foot part 1: a continuum framework for evaluating soft tissue stiffening in the pathologic foot. *Int J Numer Methods Biomed Eng.* 28(10):1056–1070. DOI:[10.1002/cnm.1494/full](https://doi.org/10.1002/cnm.1494/full).
- Gefen A, Megido-Ravid M, Itzhak Y, Arcan M. **2000.** Biomechanical analysis of the three-dimensional foot structure during gait: a basic tool for clinical applications. *J Biomech Eng.* 122(6):630–639.
- Guiotto A, Sawacha Z, Guarneri G, Avogaro A, Cobelli C. **2014.** 3D finite element model of the diabetic neuropathic foot: a gait analysis driven approach. *J Biomech.* 47(12):3064–3071. DOI:[10.1016/j.jbiomech.2014.06.029](https://doi.org/10.1016/j.jbiomech.2014.06.029)
- Jan YK, Lung CW, Cuadres E, Rong D, Boyce K. **2013.** Effect of viscoelastic properties of plantar soft tissues on plantar pressures at the first metatarsal head in diabetics with peripheral neuropathy. *Physiol Meas.* 34(1):53–66. <http://www.ncbi.nlm.nih.gov/pubmed/23248175>.
- Lemmon D, Shiang TY, Hashmi A, Ulbrecht JS, Cavanagh PR. **1997.** The effect of insoles in therapeutic footwear – a finite element approach. *J Biomech.* 30(6):615–620.
- Neptune RR, Wright IC, Den Bogert AJV. **2000.** A method for numerical simulation of single limb ground contact events: application to heel-toe running. *Comput Methods Biomed Eng.* 3(4):321–334.
- Oosterwaal M, Telfer S, Tørholm S, Carbes S, van Rhijn LW, Macduff R, Meijer K, Woodburn J. **2011.** Generation of subject-specific, dynamic, multisegment ankle and foot models to improve orthotic design: a feasibility study. *BMC Musculoskelet Disord.* 12:256–265.
- Sawacha Z, Cristoferi G, Guarneri G, Corazza S, Donà G, Denti P, Facchinetto A, Avogaro A, Cobelli C. **2009.** Characterizing multisegment foot kinematics during gait in diabetic foot patients. *J Neuroeng Rehabil.* 6:37–47.
- Sawacha Z, Guarneri G, Cristoferi G, Guiotto A, Avogaro A, Cobelli C. **2012.** Integrated kinematics-kinetics-plantar pressure data analysis: a useful tool for characterizing diabetic foot biomechanics. *Gait Posture.* 36(1):20–26. DOI:[10.1016/j.gaitpost.2011.12.007](https://doi.org/10.1016/j.gaitpost.2011.12.007)
- Sherman MA, Seth A, Delp SL. **2011.** Simbody: multibody dynamics for biomedical research. *Procedia IUTAM.* 2:241–261.
- Singh N, Armstrong DG, Lipsky BA. **2005.** Preventing foot ulcers. *J Am Med Assoc.* 293(2):217–228.
- Thelen DG, Anderson FC. **2006.** Using computed muscle control to generate forward dynamic simulations of human walking from experimental data. *J Biomech.* 39:1107–1115.
- van Schie CHM. **2005.** A review of the biomechanics of the diabetic foot. *Int J Low Extrem Wounds.* 4(3):160–170.
- Wild S, Roglic G, Green A, Sicree R, King H. **2004.** Global prevalence of diabetes: estimates for the year 2000 and projections for 2030. *Diabetes Care.* 27(5):1047–1053.
- Wright IC, Neptune RR, van den Bogert A, Nigg B. **1998.** Passive regulations of impact forces in heel-toe running. *Clin Biomech.* 13:521–531.
- Yamaguchi GT, Zajac FE. **1989.** A planar model of the knee joint to characterize the knee extensor mechanism. *J Biomech.* 22(1):1–10.
- Yarnitzky G, Yizhar Z, Gefen A. **2006.** Real-time subject-specific monitoring of internal deformations and stresses in the soft tissues of the foot: a new approach in gait analysis. *J Biomech.* 39(14):2673–2689.